EFFECT OF DEFORMATION ROUTES ON THE EFFICIENCY OF THE RADIAL-SHEAR ROLLING PROCESS

Sergey Lezhnev[1], Evgeniy Panin[2], Abdrakhman Naizabekov[3], Alexandr Arbuz[4], Dmitry Kuis[5], Fedor Popov[4], Pavel Tsyba[1], Elena Shyraeva[6]

[1]*Rudny Industrial University, Rudny, Kazakhstan, sergey_legnev@mail.ru (S.L.); tpl-work@mail.ru (P.T.)*
[2]*Karaganda Industrial University, Temirtau Kazakhstan, ye.panin@tttu.edu.kz (E.P.)*
[3]*Science, Education and Staff Planning LLP Astana, Kazakhstan, naizabekov57@mail.ru (A.N.)*
[4]*Nazarbayev University, Astana Kazakhstan, zubra_kz@mail.ru (A.A.); f.popov@tttu.edu.kz (F.P.)*
[5]*Belarusian State Technological University Minsk, Belarus, dmitrykuis@mail.ru (D.K.)*
[6]*Nosov Magnitogorsk State Technical University Magnitogorsk, Russia, e.shyraeva@mail.ru (E.S.)*

Received 03 February 2026
Accepted 21 March 2026
DOI: 10.59957/jctm.v61.i3.2026.17

ABSTRACT

The paper presents the simulation of the radial-shear rolling process in two technological routes. The direct route involved the repeated rolling of the workpiece in the second pass. In the reverse route, the rolls were rotated in the opposite direction in the second pass, and the workpiece was captured at the exit from the rolls. The analysis of the shape change showed that the reverse rolling process resulted in the complete rolling over of the helical surface formed in the first pass. The analysis of the stress-strain state and the microstructure evolution revealed that the direct rolling process resulted in a gradient structure with fine grains on the bar surface and elongated grains in the axial zone, while the reverse rolling process allowed for a more uniform distribution of grain size across the cross-section. Additionally, it was found that the reverse rolling route allowed for a greater processing of the axial zone due to the deeper penetration of plastic deformation into the workpiece. The final choice of the deformation route will depend on the desired outcome, whether it is a uniform or gradient structure across the bar.

Keywords: radial-shear rolling, modeling, deformation routes, stress-strain state, Cellular Automata, FEM.

INTRODUCTION

It has long been proven that ultrafine-grained materials (metals and alloys) have broad prospects for their practical use in various industries due to their "excellent" mechanical properties. In practice, ultrafine-grained materials can be obtained using various methods of pressure processing, which allow for the implementation of severe plastic deformation (SPD) throughout the entire volume of the deformed metal [1]. SPD implementation is one of the most important conditions for the formation of an ultrafine-grained structure and for obtaining a metal with the necessary level of properties: increased strength while maintaining or slightly reducing ductility. This combination of properties is due to the equiaxed shape of the grains and the special state of the grain boundaries, which have a large number of grain boundary dislocations and contribute significantly to the overall deformation mechanism.

If we focus on the machine-building industry, it is still the case that most metal materials used in

this industry have a coarse-grained structure. This is despite the advantages of using metals and alloys with an ultrafine-grained structure. This is primarily due to the fact that most of the developed methods of pressure processing that implement intensive plastic deformations and allow for the production of metals and alloys with an ultrafine-grained structure are technically and/or economically inefficient for use in small-scale production. For example, the well-known and studied SPD method of equal-channel angular pressing (ECAP) has a number of disadvantages and allows for the production of only small-sized workpieces, which has led to its use for obtaining metals and alloys with an ultrafine-grained structure only in experimental studies and occasionally in industrial production for one-off items [2]. The existing more technologically advanced combined SPD methods, such as "rolling-ECAP", "ECAP-drawing", Conform, which allow for the production of long-sized products with an ultrafine-grained structure, have also not found widespread use in industry due to their complexity and high cost [3 - 5]. This is why rotational forging and radial-shear rolling are still the simplest and most promising methods of implementing severe plastic deformation in long-sized products [6, 7].

Radial-shear rolling (RSR) is a helical rolling process using a three-roll scheme, but with one difference: it uses an increased feed angle, which lies in the range of α = 18 - 20° at a conventional rolling angle of β = 5° [7]. This ensures that the strongest vortex deformations develop in the metal from the surface of the workpiece to its center, preventing the appearance of tensile stresses in the axial part of the workpiece. Additionally, the main feature of the RSR process in terms of structure modification is the preferential formation of a fine-grained equiaxed structure on the periphery of the sample and an elongated oriented texture in the axial zone [8 - 10]. This property allows the process to be used as a tool for gradient modification of the metal structure. Based on this deformation scheme, a number of rolling mills for radial-shear rolling of solid round workpieces have been developed and put into small-scale production [11]. In most cases, these rolling mills have a common design scheme and differ only in terms of the size of the workpieces they roll. However, in some cases, these mills also have design differences, such as in the geometry of the working rolls shown in Fig. 1, which affects the characteristics of the deformation process. For example, the rolls of the RSR 10-30 mill (Fig. 1a), are designed for standard deformation, while the rolls of the SVP-08 mill (Fig. 1b), allow for both standard and reverse deformation of workpieces [12, 13].

Previously, based on computer modeling, a comparative analysis of the deformation process of billets on two RSR mills (RSR 10-30, SVP-08), which have different designs of working rolls, and its influence on a number of indicators, such as shape change, stress-strain state, energy-power parameters, and others, was carried out [14]. Based on this analysis, the advantages and disadvantages of using the rolls shown in Fig. 1 were identified. As mentioned above, the rolls shown in Fig. 1b can provide both standard and reverse deformation of billets on the RSR mill. The analysis of scientific, technical, and patent literature showed that there is currently no information about a comparative analysis of these deformation schemes (standard and reverse) of billets on the RSR mill on the above-mentioned indicators, as well as on the microstructure evolution.

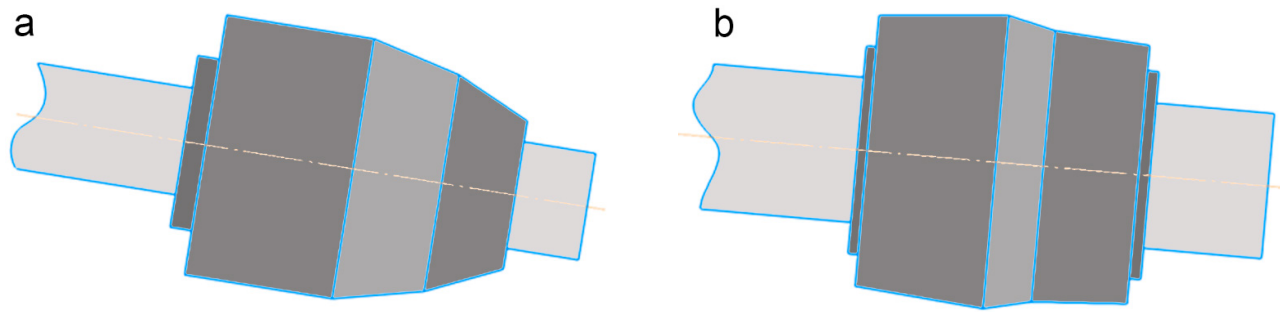

Fig. 1. Geometry of rolls of radial-shear rolling mills: (a) RSR 10-30; (b) SVP-08.

In our opinion, this is a missed opportunity, as it is the correct choice of geometric and technological parameters of metal deformation on the RSR mill that allows for the production of high-quality rods with an ultrafine grain structure and a specified level of properties with fewer passes. The use of the reverse scheme is both a geometric parameter, as it changes the shape of the deformation zone during an even pass, and a technological parameter, as it changes the direction of metal flow during an even pass. Therefore, the purpose of this work is to use computer modeling to conduct a comparative analysis of the deformation process of billets on a radial-shear rolling mill using a traditional and reverse scheme.

EXPERIMENTAL

The DEFORM program was used for finite element modeling of the radial-shear rolling process. The geometry of the rolls corresponded to the actual design of the SVP-08 mill rolls (Fig. 1b). The initial diameter of the workpiece was 30 mm, and the length of the workpiece was 150 mm. The rolling process was performed to a diameter of 28 mm in the first pass and to a diameter of 26 mm in the second pass.

AISI 1010 steel was selected as the workpiece material. The rheological properties of the workpiece material were taken from the internal DEFORM material database. The following technological parameters were used in the computer modeling of the process:

- the type of workpiece material was isotropic and elastoplastic; the type of roll material was rigid;

- the type of finite elements was tetrahedral; the number of finite element nodes was 72524, and the number of finite elements was 338677; the density of finite elements in areas with complex geometry was 6 (the volume of elements in the surface layer was 6 times smaller than in the rest of the workpiece);

- the rolling process was performed at an ambient temperature of 20°C;

- the temperature of the workpiece before rolling was 1100°C;

- the calculation type was non-isothermal; the heat transfer coefficient between the workpiece and the tool was 5000 W m^{-2} $°C^{-1}$;

- the heat transfer coefficient between the workpiece and the environment was 20 W m^{-2} $°C^{-1}$;

- the contact interaction between the workpiece and the rolls was modeled using the Siebel friction model. To create the most rigid grip conditions, the coefficient of friction between the metal and the rolls was set to 0.5 (which corresponds to a rough surface with a high level of roughness and no lubrication);

- the rotational speed of the rolls was 50 rpm;

- the feed angle was 20°, and the inclination angle was 7°.

The calculation was performed using a direct iterative method and a sparse matrix solver to improve the convergence rate at each step. To ensure high accuracy, a time increment of 0.001 seconds was used in the calculation.

RESULTS AND DISCUSSION

Fig. 2 shows the shape changes of the workpiece. After each pass, distinct helical traces remain on the workpiece surface due to the translational-rotational motion of the workpiece during radial-shear rolling. At this stage, there are already noticeable differences in the deformation routes. In the case of direct rolling, the helical groove on the second pass exactly matches the location of the coils after the first pass (Fig. 2a, b). In this case, there are five coils on the simulated workpiece. In the case of reverse rolling, the workpiece is fed from a diameter of 80 mm instead of 86 mm (as in the case of direct rolling). This allows the workpiece to fully roll over the surface area to reach a maximum diameter of 90 mm. As a result, the workpiece exhibits a new helical surface with fewer coils (Fig. 2c).

The analysis of the strain state confirms this fact. Fig. 3 shows the distribution patterns of the equivalent strain, which is determined by Eq. (1):

$$\varepsilon_{EQV} = \frac{\sqrt{2}}{3}\sqrt{(\varepsilon_1-\varepsilon_2)^2+(\varepsilon_2-\varepsilon_3)^2+(\varepsilon_3-\varepsilon_1)^2} \quad (1)$$

where ε_1 , ε_2 , ε_3 - principal strains.

On the workpiece surface during direct rolling, clear helical deformation zones are visible, with the maximum values occurring in the depressions, reaching a value of 7, while the strain value on the coils is about 5.5 (Fig. 3a). During reverse rolling, it is clearly visible that the overall strain level is lower, with the equivalent strain reaching a value of 5.8 in the depressions, while the

strain value on the coils is about 5 (Fig. 3b).

At first glance, due to the stricter rolling conditions in the reverse route, the processing in reverse rolling should be higher. However, a further examination of the strain state in the longitudinal section provides an explanation for this paradox (Fig. 3c-d). Here, the distribution of strain is opposite - in reverse rolling, the entire workpiece section receives a higher level of strain, especially in the axial zone, which traditionally receives minimal processing. This can be explained by the fact that in reverse rolling, the cross-section of the workpiece receives a higher level of compression due to the complete rolling of the initial helical surface after 1 pass. As a result, this contributes to a more intense penetration of plastic deformation into the workpiece. In direct rolling, the conditions are softer, so the central zone is less processed, while the surface zone is more intensively processed.

To confirm this hypothesis, the stress state was studied from two perspectives. First, the equivalent stress parameter (stress intensity) was examined, which is defined by Eq. (2):

$$\sigma_{EQV} = \frac{1}{\sqrt{2}}\sqrt{(\sigma_1-\sigma_2)^2+(\sigma_2-\sigma_3)^2+(\sigma_3-\sigma_1)^2} \quad (2)$$

where σ_1, σ_2, σ_3 - principal stresses.

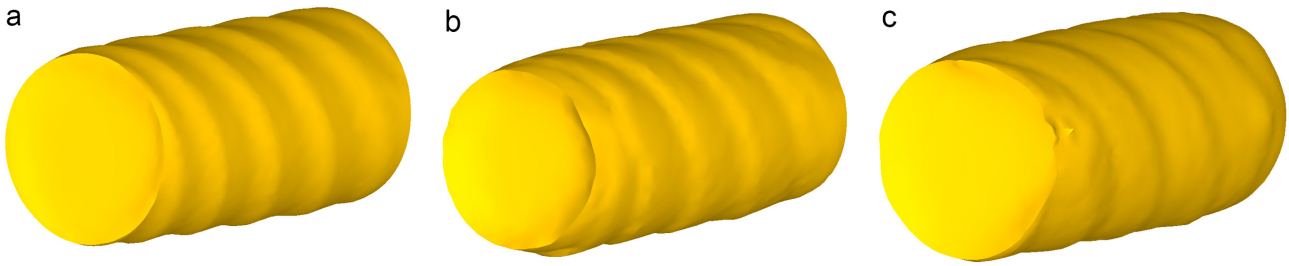

Fig. 2. Shape of the workpiece: (a) after the first pass; (b) after the second pass of direct rolling; (c) after the second pass of reverse rolling.

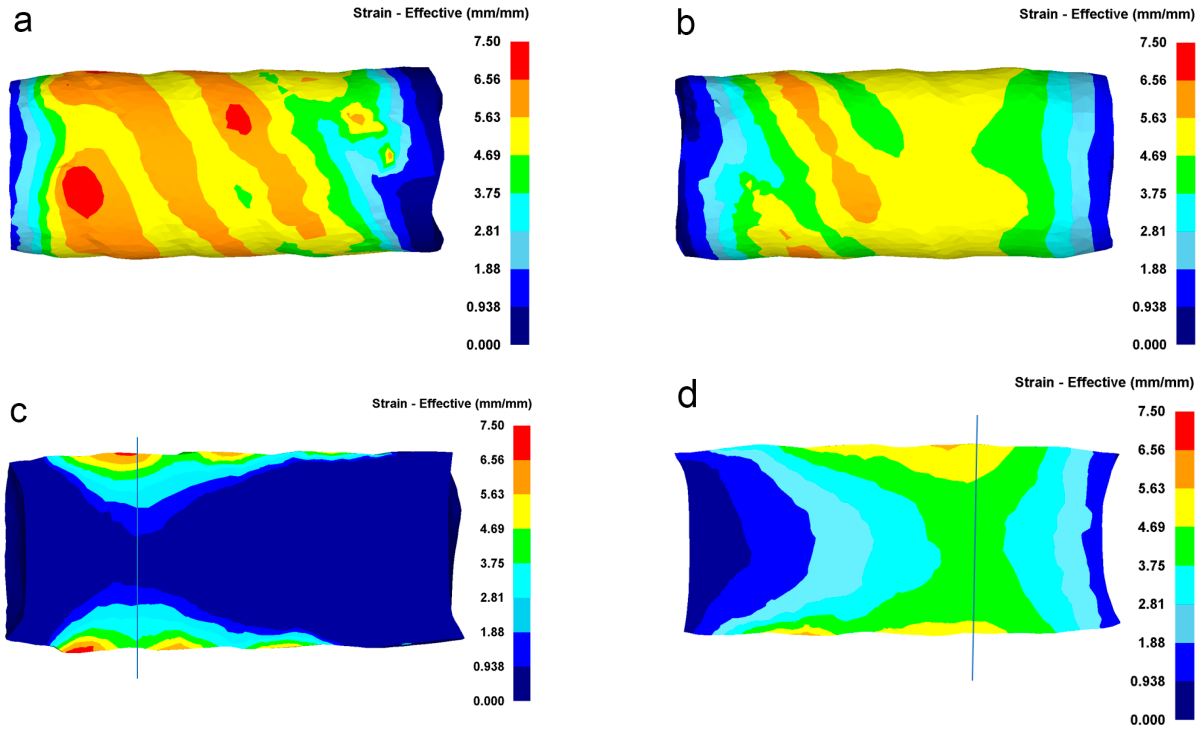

Fig. 3. Equivalent strain: (a) surface, direct rolling; (b) surface, reverse rolling; (c) longitudinal section, direct rolling; (d) longitudinal section, reverse rolling.

As a sub-root expression, its value is always positive. The physical meaning of this parameter is that it shows the average effect of all possible stresses, which is essentially their intensity. When considering this parameter, it becomes clear why such contradictory results were obtained for the strain state. Despite having the same numerical value, which primarily depends on the workpiece material and its temperature, there is a significant difference in terms of the distribution of stresses in the workpiece cross-section. During direct rolling, due to the deformation along a fixed trajectory of a helical profile, the overall level of stresses is relatively low and covers approximately half of the workpiece's diameter, while the central zone remains relatively unloaded, with an equivalent stress level of no more than 43 MPa (Fig. 4a). In contrast, during reverse rolling, due to the more severe deformation conditions, the stress concentrations cover almost the entire cross-section of the workpiece, with an equivalent stress level in the axial zone reaching 85 MPa, which is twice as high as during direct rolling (Fig. 4b). Therefore, reverse rolling allows for a greater processing of the axial zone of the workpiece due to the deeper penetration of plastic deformation, which is facilitated by the extended nature of the stress concentrations across the cross-section of the rod.

Consideration of the average hydrostatic pressure makes it possible to confirm this effect most accurately. Its value is determined by Eq. (3):

$$\sigma_{AV} = \frac{\sigma_1 + \sigma_2 + \sigma_3}{3} \quad (3)$$

where σ_1, σ_2, σ_3 - principal stresses.

Since, unlike the previously considered equivalent stress, there is no square root here, the value of the average hydrostatic pressure can take both positive and negative values. The physical meaning of this parameter is to determine the prevailing type of load at a specific point - whether it is tension or compression. For a comparative analysis of this parameter, it is crucial to present all the results on the same scale. As a result, the obtained patterns of the average hydrostatic pressure distribution fully confirm the previously obtained results. In the area of direct contact between the metal and the rolls, there are zones of compressive stress, reaching a value of -530 MPa in both cases. However, the central zone of the workpiece experiences a completely different effect. During direct rolling, there are tensile stresses, reaching a value of 120 MPa directly in the axial zone (Fig. 5a). This is a classic distribution of stresses during rolling, where a multi-pass rolling process results in an ultrafine-grained structure on the surface and large elongated grains (rolling texture) in the center.

During reverse rolling, almost the entire cross-section is subjected to compressive stresses. In the axial zone, where the level of compressive stresses is traditionally minimal, the stress reaches -30 MPa (Fig. 5b). This effect contributes to a deeper penetration of plastic deformation from the surface to the axial zone of the bar.

To complete the analysis of the stress-strain state, it was decided to use the Lode-Nadai coefficient. This coefficient allows for an assessment of the nature

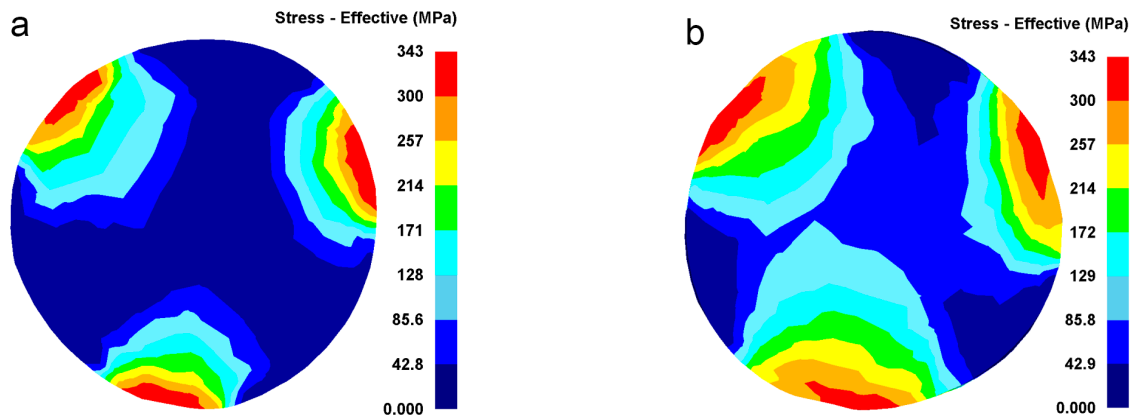

Fig. 4. Stress intensity in the workpiece section: (a) direct rolling; (b) reverse rolling.

of the deformation occurring in the workpiece, i.e., determining the type of deformation at a specific point: tension, compression, or shear. The coefficient value ranges from -1 to 1. A coefficient value approaching 1 corresponds to compression, while a coefficient value approaching -1 corresponds to tension. A coefficient value approaching 0 corresponds to shear.

The Lode-Nadai coefficient is calculated using Eq. (4):

$$\mu = 2 \cdot \frac{\varepsilon_2 - \varepsilon_3}{\varepsilon_1 - \varepsilon_3} - 1 \quad (4)$$

where ε_1 , ε_2 , ε_3 - principal strains.

To analyze this parameter, the cross-sections shown in Fig. 3 were examined. Measurements of the principal strains were taken in the vertical cross-sections corresponding to the maximum penetration of deformation into the workpiece (indicated by the lines). To do this, the internal DEFORM tool "Parameter between two points" was used in this section, which creates equidistant 20 points between the initial and final marks by default, which is an effective approach for measuring the parameters in a specific section. The results are presented in Fig. 6, the X-axis shows 20 points for measuring the principal strain components, and the Y-axis shows the dimensionless values of the Lode-Nadai coefficient.

The results of the Lode-Nadai coefficient definitively confirm the hypothesis that reverse rolling contributes to a higher processing of the rod in the axial zone. During direct rolling, the surface layers of the workpiece (points 1 - 4 and 17 - 20) undergo predominantly shear deformation, as the coefficient value ranges from 0.15 to -0.2 (i.e., as close to 0 as possible). As the workpiece moves deeper into the axial zone, the nature of the deformation changes, and a distinct tensile effect is observed in the axial zone, with the coefficient value reaching -0.7. During reverse rolling, the coefficient value in the surface layers reaches 0.4, indicating a higher degree of compression deformation. As the workpiece moves deeper into the axial zone, the nature of the deformation remains similar, but the level of tensile deformation is significantly lower. The maximum value in the axial zone increases from -0.7 to -0.3, which is a result of the broader compressive stress zones encompassing the axial zone and reducing the level of tensile stress that inevitably occurs during reverse rolling.

In addition to studying the stress-strain state parameters, it is important to investigate the forces generated on the deforming tools. If these forces exceed critical levels, it can lead to equipment failure. Therefore, when selecting the most optimal conditions from several options, the option with the lowest force is often chosen. Fig. 7 shows the summary graphs of force distribution for both routes. For both routes, the force graphs have a stable level without frequent jumps in values. Individual jumps characterize the restructuring of the finite element mesh not in the local deformation zone, but throughout the entire workpiece volume. These jumps in the force graphs are considered to be within the acceptable error of the finite element method and should not be taken into account. During the first pass, the force graphs are identical, with a force level of approximately 58 kN. During the second pass, the overall force level is

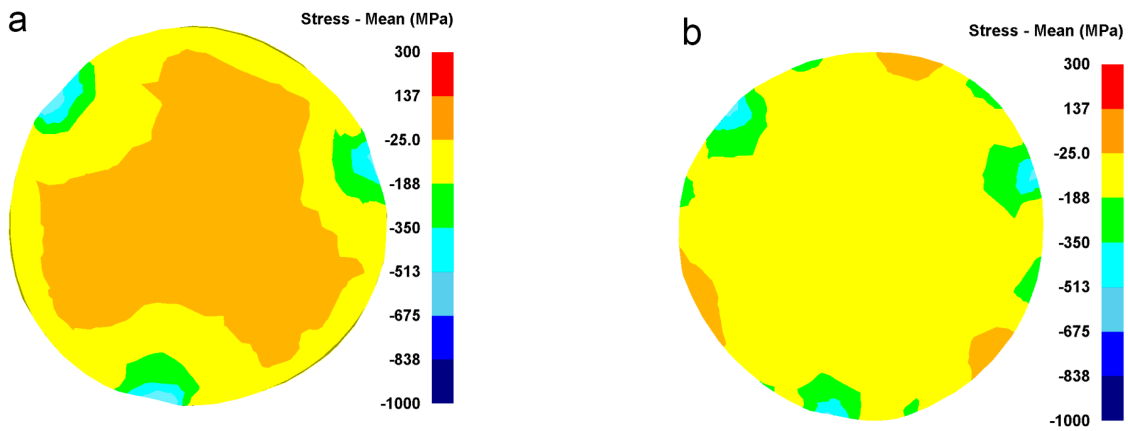

Fig. 5. Average hydrostatic pressure in the workpiece section: (a) direct rolling; (b) reverse rolling.

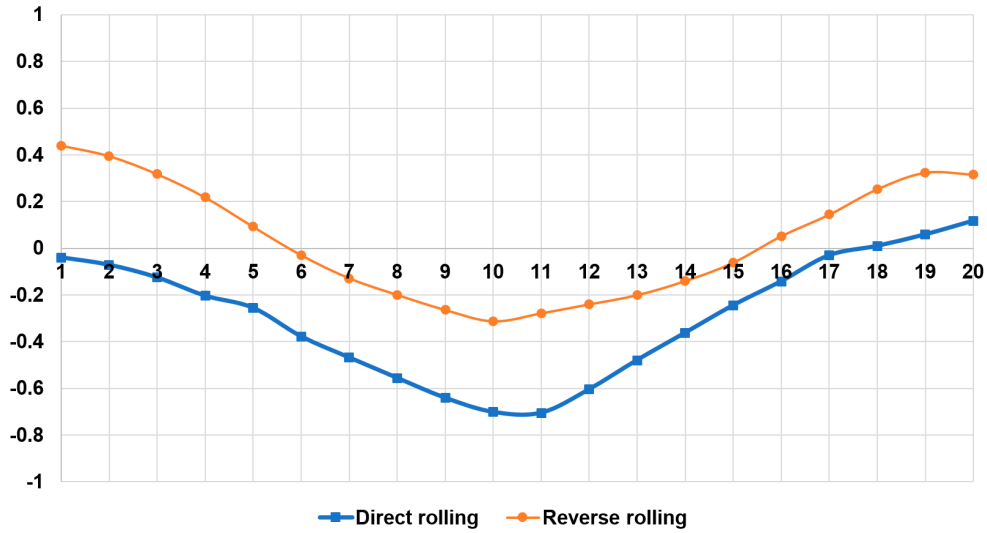

Fig. 6. Lode-Nadai coefficient for different routes.

approximately the same, at 96 kN. However, the length of the graphs is of interest. During direct rolling, the workpiece experiences fewer issues with gripping and rolling, as the deformation follows the same helical route. In contrast, during reverse rolling, the overall deformation time increases due to the braking of the workpiece in the rolls, resulting in the formation of a new helical profile. As a result, the total length of the two passes increases from 4 to 11.5 s, despite the absence of any technological operations between the passes.

After studying the stress-strain state and energy-force parameters, it is recommended to study the microstructure evolution during the implementation of the considered radial-shear rolling schemes. The classical JMAK method is not capable of recording changes in the shape of the initial grain, but the Cellular Automata method is capable of doing so. However, this method has a disadvantage in that it only allows the study of the microstructure at predetermined points. Given this, it was decided to use the Cellular Automata method in this study to obtain data on both the size and shape of the grains. To use this method, it is necessary to initially determine the points on the workpiece where the structure will be modeled.

When studying the stress-strain state parameters, it was found that the level of strain increases most intensively in the surface and peripheral zones, while the central zone is less affected. Therefore, three points were selected: on the surface (0.5 mm from the edge), in the peripheral zone of the cross-section (0.4 of the radius, in the direction from the surface to the center), and directly in the center.

The Cellular Automata algorithm uses the calculated stress-strain state, deformation rate, and temperature data from the DEFORM model, supplementing it with data on the physical and chemical properties and their behavior for the specified material and its structure. According to the Yada algorithm, it calculates the parameters of the static and dynamic recrystallization processes, which affect the change in grain size, and the application of the deformation-velocity scheme affects the change in grain shape [15]. The algorithm uses a large number of model coefficients, which are specific to different materials and deformation modes. These coefficients are discussed in detail by Lenard et al., where a large number of values for these coefficients are presented for various steel and alloy grades, depending on the types of deformation and thermal treatments [16]. To display the simulation results, the window settings were set to a square format with dimensions of 150 by 150 μm. The initial structure of the metal in the annealed state was set to an equiaxed arrangement of grains with an average size of 40 μm (Fig. 8).

Fig. 9 - 10 show the results of modeling the microstructure evolution at selected points for the two deformation routes. It can be noted that each technology has its own advantages. The direct route of the radial-shear rolling results in a gradient structure with a finer

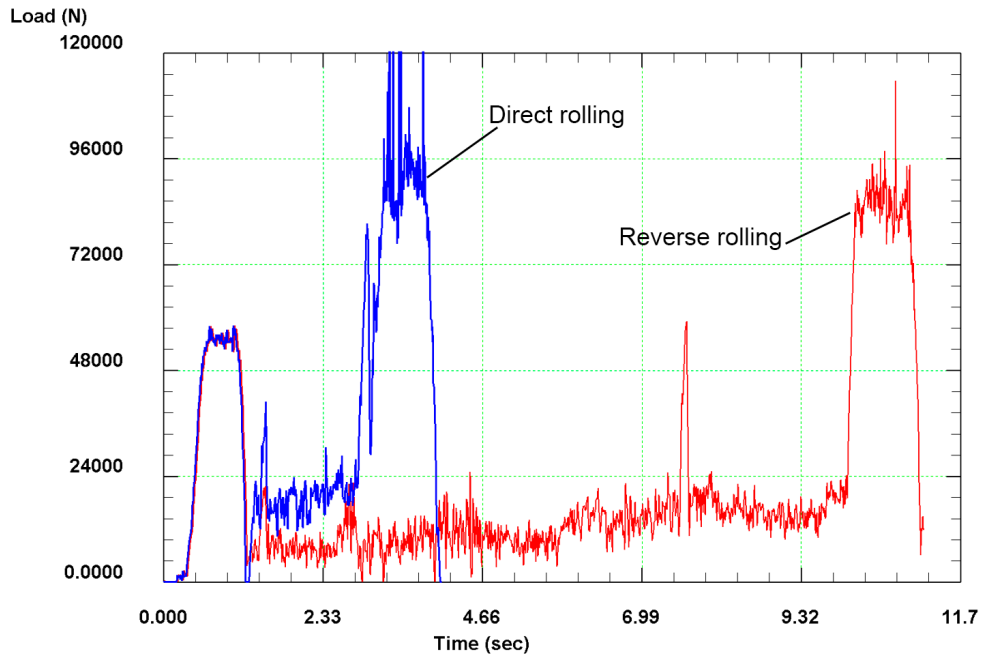

Fig. 7. Deformation force at different routes.

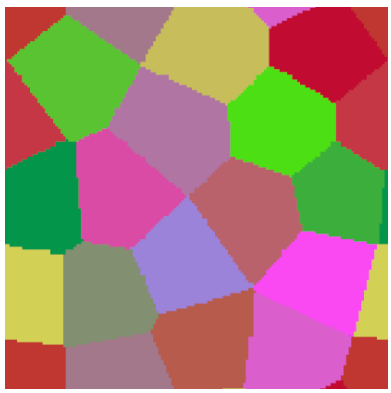

Fig. 8. Initial microstructure.

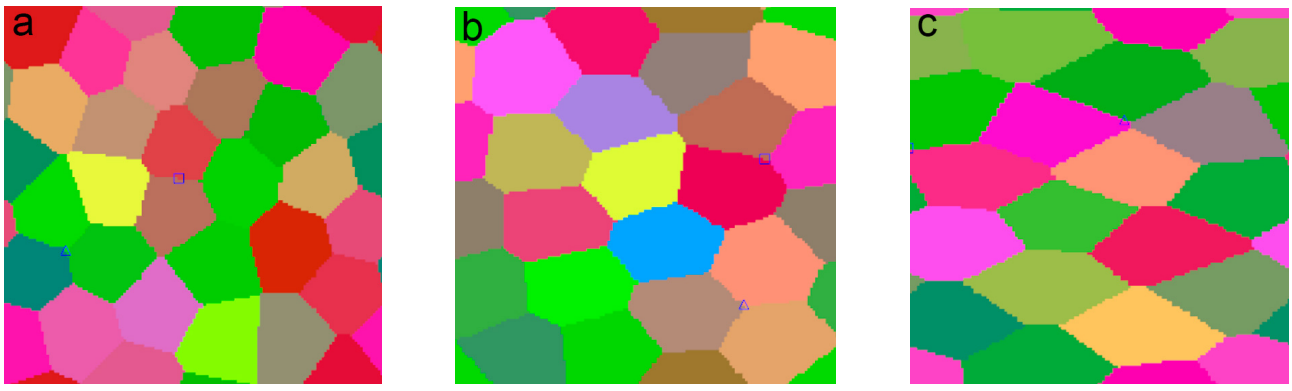

Fig. 9. Microstructure after the radial-shear rolling by direct route: (a) surface; (b) periphery; (c) center.

grain size on the bar surface and an elongated grain size in the axial zone. On the other hand, the reverse route of the radial-shear rolling results in a more uniform structure with a less refined grain size on the surface and an elongated grain size in the axial zone.

Table 1 provides the values of the average grain diameter. It can be seen that the average grain size between the surface and the center in the considered models differs by more than two times. In the case of the direct route, the difference is 22 %, while in the case of the reverse route, it is only 10 %.

Table 1. Values of the average grain diameter, μm.

Rolling model	Surface	Periphery	Center
Radial-shear rolling by direct route	30	35	39
Radial-shear rolling by reverse route	33	36	37

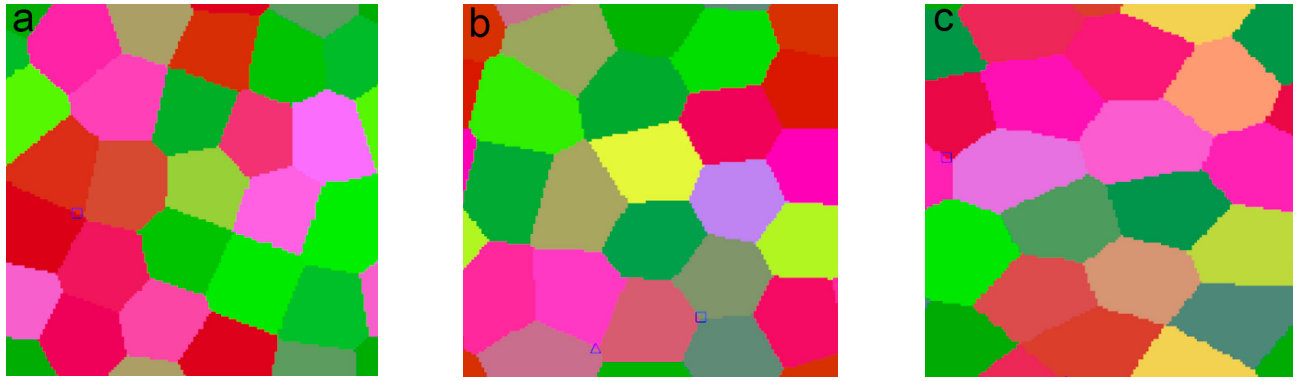

Fig. 10. Microstructure after the radial-shear rolling by reverse route: (a) surface; (b) periphery; (c) center.

CONCLUSIONS

The simulation of the radial-shear rolling process in two technological routes allowed to make the following conclusions: 1) during reverse rolling, the helical surface formed in the first pass is completely rolled over, resulting in a deeper penetration of plastic deformation into the workpiece; 2) the analysis of the stress-strain state parameters showed that the direct deformation route creates a classic metal flow, with shear deformation prevailing on the surface and tensile stresses dominating in the axial zone, causing grain elongation. The reverse route creates additional compression deformations on the surface, which reach the axial zone, thereby reducing the level of tensile stresses; 3) the analysis of the microstructure evolution confirmed the above-described results, revealing that reverse rolling produces a more uniform structure across the bar's cross-section; 4) the analysis of the deformation forces showed almost identical values, indicating that either route can be implemented on the SVP-08 mill.

Acknowledgements

This research was funded by the Science Committee of the Ministry of Science and Higher Education of the Republic of Kazakhstan (Grant № AP26100119).

Authors' contributions

S.L.: investigation, funding acquisition, project administration; E.P.: investigation, writing - original draft; A.N.: methodology; A.A.: conceptualization, methodology, investigation; D.K.: writing - review & editing; F.P.: validation, data curation, software; P.T.: visualization, investigation; E.S.: resources, formal analysis.

REFERENCES

1. R.Z. Valiev, I.V. Alexandrov, Nanostructured materials obtained by intensive plastic deformation, Moscow, Logos, 2000, (in Russian).
2. Ü. Şimşek, C. Çoğun, An investigation of the performance of equal channel angular pressed copper electrodes in electric discharge machining, Crystals, 15, 10, 2025, 849.
3. A. Naizabekov, S. Lezhnev, E. Panin, I. Volokitina, A. Arbuz, T. Koinov, I. Mazur, Effect of combined rolling - ECAP on ultrafine-grained structure and properties in 6063 Al alloy, J. Mater. Eng. Perform., 28, 1, 2019, 200-210.
4. S. Lezhnev, A. Naizabekov, A. Volokitin, I. Volokitina, E. Panin, M. Knapinski, Development and research of combined process of "equal channel angular pressing - drawing", J. Chem. Technol. Metall., 52, 2, 2017, 172-179.
5. D.A. Aksenov, A.G. Raab, N.A. Enikeev, R.Z. Valiev, Significance of the Martensitic State of Ti Grade 4 in the Evolution of Microstructure and Mechanical Properties Induced by ECAP-Conform, J. Mater. Eng. Perform., 2025 (Early Access). https://doi.org/10.1007/s11665-025-12549-9
6. S. Yang, Y. Zhou, H. Wu, Y. Shan, C. Ge, J. Du, L. Zhao, R. Yang, Z. Zhu, X. Gao, W. Long, K. Sun, Y. Zhao, K. Song. Achieving 1.2 GPa tensile strength in Cu-15Ni-8Sn alloy via large-strain rotary swaging: Multi-scale microstructure evolution and strengthening mechanisms, Mater. Sci. Eng., A, 948, 2025, 149375.
7. A. Alhaj Ali Mahmoud, Y.V. Gamin, A.N. Khakimova, T.Y. Kin, S.P. Galkin, Influence of temperature of radial-shear rolling on the structure of VT3-1 alloy, Metallurgist, 69, 2025, 121-131.
8. Y.V. Gamin, S.P. Galkin, A.N. Koshmin, A. Alhaj Ali Mahmoud, X.D. Nguyen, High-reduction radial shear rolling of aluminum alloy bars using custom-calibrated rolls, Int. J. Mater. Form., 17, 2024, 63-74.
9. Y.V. Gamin, A.N. Koshmin, A.P. Dolbachev, S.P. Galkin, A.S. Aleschenko, M.V. Kadach, Studying the Influence of Radial-Shear Rolling on Thermal Deformation Conditions of A1050 Processing, Russ. J. Non-ferr. Met., 61, 2020, 646-657.
10. A.S. Arbuz, A.B. Naizabekov, S.N. Lezhnev, F.E. Popov, N.A. Lutchenko, E.A. Panin, Experience in applying radial-shear rolling to improve the structure and properties of ferrous and non-ferrous metals and alloys, Chernye Metally, 2025, 10, 2025, 28-45.
11. S.P. Galkin, Radial shear rolling as an optimal technology for lean production, Steel in Translation, 44, 1, 2014, 61-64.
12. S.P. Galkin, Y.V. Gamin, A.S. Aleshchenko, B.A. Romantsev, Modern development of elements of theory, technology and mini-mills of radial-shear rolling, Chernye Metally, 2021, 12, 2021, 51-58.
13. S.P. Galkin, E.A. Kharitonov, Reversible radial shear rolling. Essence, opportunities, advantages, Titanium, 1, 2003, 39-45, (in Russian).
14. S. Lezhnev, A. Naizabekov, A. Tolkushkin, E. Panin, D. Kuis, A. Arbuz, P. Tsyba, E. Shyraeva, Choosing the design of a radial-shear rolling mill for obtaining a screw profile, Modelling, 5, 2024, 1101-1115.
15. H. Yada, N. Matsuzu, K. Nakajima, K. Watanabe and H. Tokita, Strength and Structural Changes under High Strain-rate Hot Deformation of C Steels, Trans. ISIJ, 23, 1983, 100-109.
16. J.G. Lenard, M. Pietrzyk, L. Cser, Mathematical and Physical Simulation of the Properties of Hot Rolled Products, Amsterdam, Elsevier, 2005.